2011 IEEE International Conference on Rehabilitation Robotics
Rehab Week Zurich, ETH Zurich Science City, Switzerland, June 29 - July 1, 2011

Passive Velocity Field Control of a Forearm-Wrist Rehabilitation Robot

Ahmetcan Erdogan and Aykut Cihan Satici and Volkan Patoglu
Faculty of Engineering and Natural Sciences
Sabancı University, İstanbul, Turkey
Email:{ahmetcan,acsatici,vpatoglu}@sabanciuniv.edu

***Abstract*—This paper presents design, implementation and control of a 3RPS-R exoskeleton, specifically built to impose targeted therapeutic exercises to forearm and wrist. Design of the exoskeleton features enhanced ergonomy, enlarged workspace and optimized device performance when compared to previous versions of the device. Passive velocity field control (PVFC) is implemented at the task space of the manipulator to provide assistance to the patients, such that the exoskeleton follows a desired velocity field asymptotically while maintaining passivity with respect to external applied torque inputs. PVFC is augmented with virtual tunnels and resulting control architecture is integrated into a virtual flight simulator with force-feedback. Experimental results are presented indicating the applicability and effectiveness of using PVFC on 3RPS-R exoskeleton to deliver therapeutic movement exercises.**

I. Introduction

Robotic devices designed for physical rehabilitation are becoming ubiquitous, since they decrease the cost of repetitive movement therapies, enable qualitative measurement of progress and promise development of novel rehabilitation protocols. Early robotic devices for upper limb rehabilitation had primarily focused on proximal joints such as shoulder and elbow, while recently the attention has been shifting towards more distal joints, such as the wrist and the hand.

In the literature, several robotic devices have been developed to target wrist rehabilitation exercises. The most commonly used wrist rehabilitation devices are developed as extension modules of task-space arm rehabilitation systems. Once such device is the wrist extension module of the *MIT-Manus* system [1], [2]. This wrist module comprises of an actuated cardan joint coupled to a curved slider and allows for 3 degrees-of-freedom (DoF) forearm-wrist movements. Another wrist module exists as a part of the *Robotherapist* upper-extremity rehabilitation support system [3]. This system is capable of controlling all forearm-wrist rotations utilizing ER actuators [4]. Another task-space rehabilitation device, *haptic knob*, has been proposed by Dovat *et al.* to target combined wrist-hand therapy [5]. *Haptic knob* is a 2 DoF back-driveable mechanism, with one rotation assigned for wrist movements [6]. Even though task-space arm rehabilitation systems are practical and simpler to implement, these devices cannot guarantee decoupled actuation and measurement of human joint motions.

Exoskeleton type rehabilitation devices are relatively more complex but can be effectively used for the implementation and measurement of targeted joint movements. There exist several upper-extremity rehabilitation systems that include forearm-wrist rotations. *Armin* and *IntelliArm* are two exoskeleton type full-arm therapy systems, which allow for forearm supination/pronation as well as the palmar/dorsal flexion of the wrist [7], [8]. These systems are also equipped with a multi-axis force sensors to collect force/torque data during therapy. *RiceWrist* is another exoskeleton designed to target physical rehabilitation of forearm-wrist motions [9], [10]. This device is of 3RPS-R kinematical structure and possesses 4 DoF [11]. With *RiceWrist*, all forearm and wrist motions can be independently controlled over their rotational axes. *RiceWrist* has also been extended to deliver full arm rehabilitation therapy, through synchronized control of this device with the *MIME* system [9].

Earlier implementations of rehabilitation robots relied on stiff position controllers that impose predetermined trajectories to patients [12]. In these controllers patient forces were viewed as disturbances and counteracted. However, clinical studies provided strong evidence that active participation of patients is crucial for increasing efficacy of robotic rehabilitation. Consequently, impedance/admittance control techniques and more recently patient-cooperative methods have been proposed to allow active participation of patients in robotic therapy [13], [14], [15], [16]. The main idea in patient-cooperative methods is to adjust the assistance provided to the patient based on patient's performance. For instance, in [17], time-optimal trajectories are calculated for point-to-point reaching tasks and tracking errors are penalized adaptively based on the deviation from the optimal trajectory. This way rehabilitation robots can "assist-as-needed", where the main contribution for a successful completion of the task is left to the patient. Unfortunately, many of the existing implementations of assist-as-needed protocols rely on minimization of trajectory tracking error, which cannot ensure that patients do not significantly deviate from the pre-determined path [18], [19]. Virtual tunnel approach is an alternative way to provide freedom to patients by allowing them to move freely as long as they do not violate the bounds defining forbidden regions. Since by merely implementing virtual tunnels cannot ensure that the tunnel is traced within a reasonable amount of time, virtual tunnels are generally augmented with a moving window that pushes the patient forward in the tunnel if he/she falls behind the pre-determined timing along the tunnel [20], [21], [22]. However,

evidence exist in motor learning literature that virtual tunnels may have negative efficacy on human learning as the participants may become dependent on existence of such assistance to complete the task [23].

In many multi degrees of freedom therapeutic path following tasks, coordination and synchronization between various degrees of freedom are imperative, while exact timing along the path is not critical. In fact, most of the time, it is preferable to let patients to complete the task at their own preferred pace. For such tasks, the contour error is the proper measure of performance. Conventional control approaches, such as assist-as-needed approaches reviewed earlier, attempt to improve path following accuracy by reducing the tracking error. However, reduction of tracking errors does not necessarily imply improvement of contour errors; in general, trajectory-based contour tracking controllers suffer from the radial reduction phenomena [18], [19]. The discrepancy between tracking error and contour error becomes more critical when humans are in the loop. In particular, even though a predetermined path defines a clinically admissible contour, trajectory tracking controllers may significantly deviate from it.

Among the available contour tracking algorithms, *passive velocity field control* (PVFC) is particularly suited for rehabilitation robotics, since this method not only minimizes the contour error but also does so by rendering the closed loop system passive with respect to externally applied forces. PVFC concept has been first proposed as a part of a smart exercise protocol in [24] and further analyzed in [25], [26]. Later, PVFC has been adapted to bilateral control [27], [28]. In [29], the controller has been further extended to include shaping of the *potential energy* of the closed loop system dynamics as well as its kinetic energy. Finally, in [30], a PVFC controller that operates solely on joint positions has been proposed, alleviating the need for velocity measurements.

In PVFC, the task to be performed and speed of the task are decoupled from each other. In particular, the task is embedded in a predefined velocity field while the speed depends on the instantaneous energy of the closed loop system. PVFC mimics the dynamics of a flywheel; hence cannot generate energy, but can store and release energy supplied to it. As a consequence, the controller renders the close-loop system passive *with respect to externally applied forces*. This is one of the unique features of PVFC approach, as classical passivity-based robot control laws [31], [32], [33] cannot guarantee passivity when external forces are considered as the input. Passivity with respect to external forces is crucial in rehabilitation, since it enhances safety by limiting the amount of energy that can be released to the patient, especially in case of an unexpected system failure.

In PVFC, speed of motion is governed by the instantaneous energy of the system; hence, can be adjusted either by changing the initial conditions of the system or through external forces (patients) doing (possibly negative) work on the system. This implies, for contour following tasks, the desired path can be traced forwards and backwards, and with different levels of assitance/resistance to the patient by simply tuning the instantaneous energy of the system through the controlled variables.

This paper presents design and control of a 3R$\underline{\text{P}}$S-$\underline{\text{R}}$ exoskeleton, specifically built for forearm-wrist rehabilitation. The mechanical design is an enhanced version of the *RiceWrist* with the following improvements undertaken along the feedback provided by therapists and patients.

- A non-symmetric 3R$\underline{\text{P}}$S-$\underline{\text{R}}$ mechanism is utilized along the palmar/dorsal flexion axis, considering different workspace and torque capabilities of human wrist about different motion axis.
- Optimal dimensional synthesis of the device is performed to maximize actuator utilization while simultaneously maximizing global isotropy and minimizing apparent inertia of the exoskeleton.
- Workspace optimization is performed considering joint limits imposed by commercial spherical joints.
- Direct-drive linear actuators are utilized to ensure high back-driveability and actuator stiffness, as necessitated by force-feedback applications.
- Ergonomy of the device is improved and the time it takes to attach/detach the exoskeleton is decreased by implementing the device with an *open* semi-circular ring design.

Moreover, kinematic and dynamics models of the device have been derived and experimentally verified. Since the task space of the exoskeleton is in $\mathbf{SO}(3) \times \mathbb{R}$, a model-based task space impedance controller with gravity compensation is implemented using quaternion error to ensure the geometrical consistency of resulting interactions. Furthermore, properly defining a potential field and an orientation error in $\mathbf{SO}(3)$, a passive velocity field controller is synthesized. All controllers are implemented on the forearm-wrist exoskeleton and experimental results are presented.

The paper is organized as follows: Section II introduces the kinematic model of human lower arm. Design of the rehabilitation device is detailed in Section III. Section IV presents PVFC controller, while, velocity field generation for the task space coordinates of the device is shown in V. Afterwards, with the help of virtual tunnels and PVFC controller, a dynamic virtual reality environment is introduced in VI. In Section VII controllers are utilized and experimental results are given. Finally, Section VIII concludes the paper.

II. Kinematics of Human Forearm and Wrist

Human forearm and wrist facilitate complex motions of the hand. In particular, neglecting the small deviations of the axes of rotation during the movement, the simplified kinematics of the human forearm and wrist can be quite faithfully modeled as a 3 DoF kinematic chain that allows supination/pronation of the forearm, flexion/extension and ulnar/radial deviation of the wrist joint with coinciding axes of rotation. Hence, unlike the reaching-type translational movements in the three dimensional Euclidian space, the the rotations of the forearm and the wrist can be more properly studied in the 3-dimensional manifold known as $\mathbf{SO}(3)$.

III. Mechanical Design of the Exoskeleton

A kinematic chain that is suitable to serve as an exoskeleton should have rotation axes of its joints coincident with the rotation axes of human wrist when the device is worn by an operator. Moreover, the choice of closed kinematic chains (parallel mechanisms) is preferable over their serial counterparts in satisfying requirements of force feedback applications, since parallel mechanisms possess inherent advantages. Specifically, parallel mechanisms offer compact designs with high stiffness and have low effective inertia since their actuators can be grounded, or placed on parts of the mechanism that experience low accelerations. In terms of dynamic performance, high position and force bandwidths are achievable with parallel mechanisms thanks to their light but stiff structure. Besides, parallel mechanisms do not superimpose position errors at joints; hence, can achieve higher precision.

In order to span an acceptable portion of the natural human wrist and forearm workspace and to ensure alignment of the axes of rotation of human joints with the controlled DoF of the device such that decoupled actuation and measurement of human joint rotations are possible, a hybrid kinematic structure, namely a 3RPS-R mechanism, is selected as the underlying kinematics of the exoskeleton. Being compact and allowing for human motions without collisions with the device, this mechanism is one of the most suitable candidates to serve as wearable force feedback device.

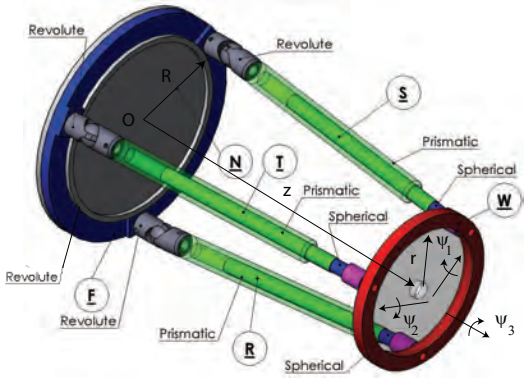

Fig. 1. Schematic representation of the 3RPS-R mechanism in perspective view.

The 3RPS-R mechanism, depicted in Figure 1, is of hybrid kinematic structure and comprises of a 3RPS parallel wrist in series with an actuated revolute (R) joint at the base platform of the wrist, as shown in Figure 1. The 3RPS platform, first introduced by Lee *et al.* [34], and further analyzed in [35], consists of five bodies: a base platform F, three extensible links R, S, T, and a moving platform W. The end-effector held by the operator is rigidly attached to the moving platform W. Extensible links are connected to the base platform via revolute joints whose axes of rotation are oriented along the tangents of F, while the moving platform is connected to the extensible links by means of spherical joints. The workspace of 3RPS-R is the product space $W = \mathbf{SO}(3) \times \mathbb{R}$. When the translational degree of freedom is adjusted to fit the specific user, the remaining workspace of the 3RPS-R mechanism lies in the Riemannian manifold $\mathbf{SO}(3)$.

The 3RPS-R mechanism was first utilized as an exoskeleton in [36] and adapted as a rehabilitation device in [9]. In [37], [38], [39], [40], dimensional synthesis of the 3RPS-R platform was studied using multi-criteria design optimization techniques. In particular, actuator utilization was optimized while simultaneously maximizing global isotropy and minimizing apparent inertia of the mechanism. Implementation of several task-space impedance and position controllers were also presented in these references.

Even though optimal dimensional synthesis of the device provide proper link lengths of the device, several other important implementation issues still remains to be considered. One such particular issue is the workspace limits introduced by the physical joint limits of spherical joints. Specifically, commercial high-precision spherical joints used for implementation of the exoskeleton possess 40° joint limits. Given this limit and the unsymmetrical design of 3RPS-R platform, a workspace optimization is needed to be performed to determine best possible configuration of the spherical joints on the device end-effector. Three objectives are watched as the outcome of a brute-force search: the total workspace volume attained, the maximum range of motion along abduction/adduction and the maximum range of motion along flexion/extension degrees of freedom. The optimization results suggest that the configuration yielding the largest workspace volume also maximizes the workspace along the flexion/extension while keeping abduction/adduction workspace to cover the human range of motion. The optimal configuration of spherical joints at the end-effector is depicted in Figure 3. Figure 2 presents the workspace of the mechanism before and after the workspace optimization is conducted. The results are sticking, as proper orientation of the spherical joints can increase the workspace of the mechanism by 50% both in unlar/radial deviation and flexion/extension DoF.

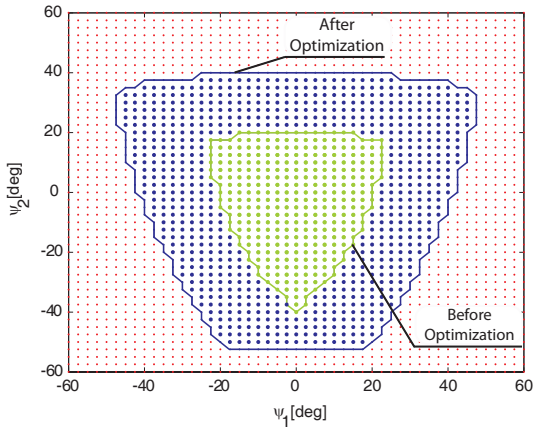

Fig. 2. Workspace coverage of 3RPS-R along ψ_1 and ψ_2 axes. It is clear that with optimization, range of motion is extended in two axes

Another important design requirement pertains to ergonomics and ease of attachment. In our design, an *open* semi-circular ring design is favored such that the patients can be attached to and de-attached from the device easily. Implementation of such an *open* ring design is made possible

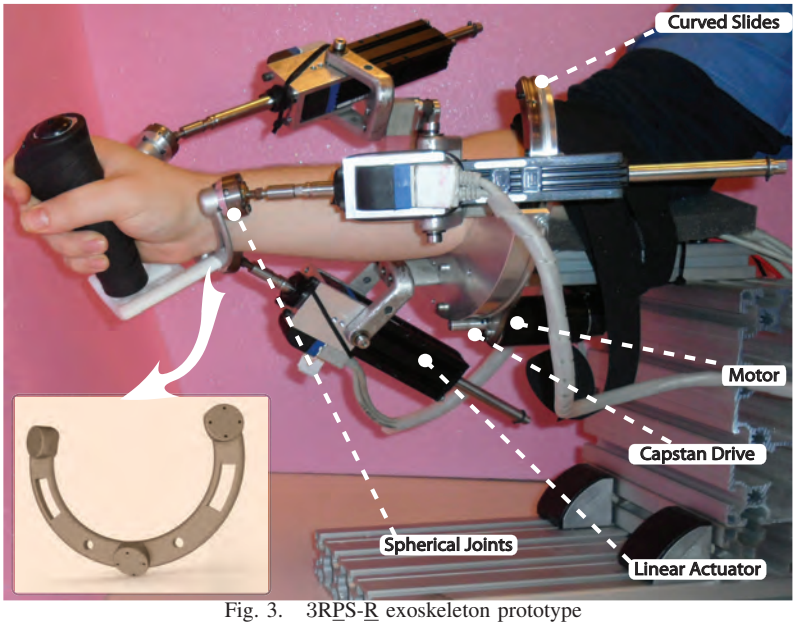

Fig. 3. 3RPS-R exoskeleton prototype

by the non-symmetrical design of the 3RPS-R mechanism, allowing for 200° arcs instead of full circles be used for the base and end-effector rings.

Other design decisions include utilization of direct-drive linear actuators at the prismatic joints to ensure high back-driveability and actuator stiffness, while using a DC motor driven capstan mechanism to actuate the base ring, since much higher torques are required for the forearm rotation compared to wrist rotations. The maximal torque values and the average apparent inertia calculated over the workspace at the end-effector are 4.984 Nm and 418.56 kg mm^2 for wrist flexion/extension, 4.000 Nm and 288.9 kg mm^2 for wrist abduction/adduction and 56.43 Nm and 37088 kg mm^2 for forearm supination/pronation, respectively. The disadvantage of hybrid approach is the asymmetry in the apparent inertia which is caused by rotating the three linear motors for forearm rotation. Future modifications are in progress in order to move this rotation to end-effector, and therefore, reduce inertia. Hollow aluminum links reinforced with honeycomb structure are used to a provide reliable but lightweight design. Finally, to maximize comfort and hygiene, critical surfaces are covered with silicon and disposable medical bands. The final prototype of the exoskeleton is presented in Figure 3. The handle is an appropriate end effector for a flight simulator, however, there exists several modules for different types of interaction including an active joint for hand grasp therapy.

IV. Passive Velocity Field Control

Given a smooth path between the current and target configurations, virtual tunnels may be employed in order to restrict large deviations of the patient from the desired path. However, for patients with limited ability to control their limbs, further assistance is required to ensure their completion of the path following task. The way that such assistance is provided is a crucial aspect of robot-assisted therapy that strongly affects its efficacy.

In this study, PVFC approach is used to provide assistance to the patients. Use of PVFC in rehabilitation robotics is advantageous in various ways: First of all, the control law ensures passivity with respect to external torque inputs, an asset no other passivity-based controllers with trajectory tracking objective can achieve. Indeed, this property of the control law ensures no harm be done on the patient should a given trajectory cannot be tracked. Specifically, given the dynamics of the manipulator defined in task space as

$$\mathrm{M}(\mathrm{q})\ddot{\mathrm{q}} + \mathrm{C}(\mathrm{q},\dot{\mathrm{q}})\dot{\mathrm{q}} = \tau + \tau_{\mathrm{e}} \tag{1}$$

where $\mathrm{M}(\mathrm{q}) \in \mathbb{R}^{n\times n}$ is the inertia matrix, $\mathrm{C}(\mathrm{q},\dot{\mathrm{q}}) \in \mathbb{R}^{n\times n}$ is the Coriolis matrix, τ represents control forces, and potential forces are embedded in the external force τ_{e}, PVFC renders the controlled manipulator as a dynamic non-linear impedance that can store and release the energy supplied to it. Thanks to this property, the control law guarantees passivity with respect to the supply rate $s(\tau_e, \dot{q}) = {\tau_{\mathrm{e}}}^T \dot{\mathrm{q}}$, that is, it ensures passivity with respect to external force inputs τ_{e}, implying

$$\int_0^t {\tau_{\mathrm{e}}}^T \dot{\mathrm{q}}\, d\tau \geq -c^2 \tag{2}$$

where c is some real number.

Secondly, the control law minimizes the "contour error" rather than the more conventional trajectory error. Minimizing the contour error, defined as the closest path (in the proper space) from the actual position of the manipulator to the desired contour, is advantageous since such a control technique guarantees minimal deviations from the desired path, while trajectory error based controllers can largely deviate from the path as the trajectory tracking error is dictated by time parametrization [41]. In particular, the desired task and the speed of task execution are decoupled in PVFC. For instance, for a contour following task, the desired path is encoded into the velocity field, so that for each location of the robot end-effector, a proper reference trajectory can be calculated,

while the controller ensures that the velocity of the robotic manipulator converges to a scaled multiple of this desired velocity in the absence of external forces: Formally, the controller guarantees that for any initial condition $(\mathrm{q}(0), \dot{\mathrm{q}}(0))$, there exists a constant $\rho > 0$ s.t.

$$\lim_{t\to\infty} \dot{\mathrm{q}}(t) - \rho \mathrm{V}(\mathrm{q}(t)) = 0. \tag{3}$$

when $\tau_{\mathrm{e}} \equiv 0$. Note that the parameter ρ dictates the speed of task execution and can be positive or negative.

Finally, in the PVFC architecture, the amount of assistance can be adjusted and same path can be traced forward and backwards, and at different speeds by simply tuning the controller parameters. Specifically, the magnitude of ρ is governed by the instantaneous energy of the system; hence, can be adjusted either by changing the initial conditions of the system or through external forces doing (possibly negative) work on the system. This implies, for contour following tasks, the desired path can be traced forwards and backwards, and at different speeds by simply tuning the instantaneous energy of the system through controlled variables.

Given a desired velocity field, the control specifications are satisfied by introduction of an extra state, which may be interpreted as the velocity of a fictitious flywheel of mass M_F that augments the original system as an extra energy storage element. Then the kinetic energy function for the augmented system is defined as

$$\bar{k}(\bar{\mathrm{q}}, \dot{\bar{\mathrm{q}}}) = \frac{1}{2} \dot{\bar{\mathrm{q}}}^T \bar{\mathrm{M}}(\bar{\mathrm{q}}) \dot{\bar{\mathrm{q}}}. \tag{4}$$

where $\bar{\mathrm{M}}$ denotes the inertia matrix of the augmented system, $\bar{q}$ and $\dot{\bar{q}}$ represent the augmented configurations and velocities, respectively. The desired velocity field is also extended to encompass the extra state such that when it (or a multiple of it) is exactly tracked, the kinetic energy of the augmented system remains constant, that is

$$\bar{k}(\bar{\mathrm{q}}, \bar{\mathrm{V}}(\bar{\mathrm{q}})) = \frac{1}{2} \bar{\mathrm{V}}(\bar{\mathrm{q}})^T \bar{\mathrm{M}}(\bar{\mathrm{q}}) \bar{\mathrm{V}}(\bar{\mathrm{q}}) = \bar{E} > 0 \tag{5}$$

Given an augmented velocity field, the skew-symmetric control law is calculated using two terms which are analogous to feed-forward dynamic compensation and a feedback term forces the error dynamics to converge as

$$\bar{\tau}(\bar{\mathrm{q}}, \dot{\bar{\mathrm{q}}}) = \underbrace{\frac{1}{2\bar{E}} (\bar{\mathrm{w}} \bar{\mathrm{P}}^{\mathrm{T}} - \bar{\mathrm{P}} \bar{\mathrm{w}}^{\mathrm{T}})}_{\text{skew symmetric}} \dot{\bar{\mathrm{q}}} + \gamma \underbrace{(\bar{\mathrm{P}} \bar{\mathrm{p}}^{\mathrm{T}} - \bar{\mathrm{p}} \bar{\mathrm{P}}^{\mathrm{T}})}_{\text{skew symmetric}} \dot{\bar{\mathrm{q}}} \tag{6}$$

where $\gamma \in \mathbb{R}$ in Eqn. (6) is a control gain, not necessarily positive, which determines the convergence rate and the sense in which the desired velocity field will be followed. In Eqn. (6), $\bar{p}$ denotes the momentum of the augmented system, while $\bar{P}$ is the desired momentum of the augmented system. The symbol $\bar{w}$ represents the inverse dynamics necessary to follow the desired velocity field. Mathematically,

$$\bar{\mathrm{p}}(\bar{\mathrm{q}}, \dot{\bar{\mathrm{q}}}) = \bar{\mathrm{M}}(\bar{\mathrm{q}}) \dot{\bar{\mathrm{q}}} \tag{7}$$

$$\bar{\mathrm{P}}(\bar{\mathrm{q}}) = \bar{\mathrm{M}}(\bar{\mathrm{q}}) \bar{\mathrm{V}}(\bar{\mathrm{q}}) \tag{8}$$

$$\bar{\mathrm{w}}(\bar{\mathrm{q}}, \dot{\bar{\mathrm{q}}}) = \bar{\mathrm{M}}(\bar{\mathrm{q}}) \dot{\bar{\mathrm{V}}}(\bar{\mathrm{q}}) + \bar{\mathrm{C}}(\bar{\mathrm{q}}, \dot{\bar{\mathrm{q}}}) \bar{\mathrm{V}}(\bar{\mathrm{q}}) \tag{9}$$

In [25], it has been proven that the skew symmetric control law coupled with the skew symmetry property of the robotic manipulators renders the closed-loop system passive with respect to external force inputs and regulates the error dynamics to zero (exponentially) in the absence of external forces. Moreover, it has been shown that the total energy in the system defined by Eqn. (4) remains constant (as long as no work is done on the system by external forces) and the rate at which the parameterized trajectory progresses is determined by the instantaneous energy of the system. The reader is referred to [25], [26], [42] for stability proofs, robustness analysis and detailed convergence characteristics of PVFC.

During physical implementations of the controller, the energy level may vary due to inevitable dissipative forces, such as friction in the joints. Under such circumstances, a nominal rate at which the parameterized trajectory progresses may be dictated by adding an exogenous signal to $\bar{\tau}$ as

$$\tau_{forced} = \varsigma \bar{P} \left(r - \frac{\bar{P}^T \dot{\bar{q}}}{2\bar{E}} \right), \quad \varsigma > 0 \tag{10}$$

where ς is a damping coefficient. It can be shown that τ_{forced} causes the velocity $\dot{\bar{q}}$ to converge to $r\bar{\mathrm{V}}$.

V. Construction of Velocity Field in $\mathbf{SO}(3)$

Even though existence of a velocity field encoding the task is a crucial part of PVFC, determination of such a velocity field is not a trivial matter. One effective method attacks the velocity field generation problem from a controls perspective and designs controllers for online generation of the vector field [42]. In particular, in [42] Li *et al.* has proposed a technique for encoding velocity fields for parametric curve tracking, based on state suspension and self-pacing. The approach is similar to use of navigation functions for path planning [43] and is implemented by introducing two new states (curve parametrization τ and its time derivative $\dot{\tau}$) to the system dynamics (called suspension) and controlling these states using properly defined error functions and potential fields. To ensure good tracking performance, $\dot{\tau}$ is continually adjusted with respect to the rate of convergence (self-pacing).

For the synthesis of PVFC for 3R<u>P</u>S-<u>R</u>, the potential function used to generate the proper velocity field is defined in $\mathbf{SO}(3)$ with a topologically consistent definition of the orientation error.[1] In particular, let the desired orientation trajectory be represented by parameterized trajectory $\mathrm{x_d} : \mathcal{I} \to \mathcal{G}$ where $\mathcal{I} \in \mathbb{R}$. The workspace of 3R<u>P</u>S-<u>R</u> is $\mathbf{SO}(3)$, with each element q identified with a 3×3 real orthogonal matrix with determinant one. $T_q\mathbf{SO}(3)$ can be identified with $\{\mathrm{q}\,\omega : \omega \in \mathbf{so}(3)\}$ where $\mathbf{so}(3)$ is the space of 3×3 skew symmetric matrices. Then an error function can be defined by

$$\mathrm{E}(\mathrm{q}, \mathrm{x_d}) = \mathrm{q}\mathrm{x_d}^{-1}(\tau) = \mathrm{q}\mathrm{x_d}^{\mathrm{T}}(\tau) \tag{11}$$

where $\mathrm{x_d} : \mathcal{I} \to \mathbf{SO}(3)$ is the parameterized trajectory. Following [44], a potential function over $\mathbf{SO}(3)$ is then defined

[1]Note that the translational motion of 3R<u>P</u>S-<u>R</u> is used to properly fit the rotation axes of the exoskeleton with the axes of wrist. Once the device is adjusted for a specific user, this motion is set to this user-specific constant value throughout the therapy.

Fig. 4. Left figure presents the flight simulator, in which the movements of the plane is coupled to the rotations of the 3RPS-R end-effector. Right figure depicts cross section of tunnel on which virtual walls and velocity field are depicted schematically.

as follows. Let $\mathrm{P} \in \mathbb{R}^{3\times3}$ be a symmetric matrix with distinct eigenvalues $\lambda_1 < \lambda_2 < \lambda_3$ and $(\lambda_1+\lambda_2)(\lambda_1+\lambda_3)(\lambda_3+\lambda_2) \neq 0$. Then,

$$U(E) = \frac{1}{\lambda'} trace\left[\mathrm{P}\left(\mathrm{I}-\mathrm{E}\right)\right] \tag{12}$$

where $\lambda' = \lambda_2 + \lambda_3 - \lambda_1$ and I is the 3×3 identity matrix defined a potential function U in $\mathbf{SO}(3)$ and $\mathrm{E} \in \mathbf{SO}(3)$ is a critical point of $U(\cdot)$. Furthermore, $\mathrm{E} = \mathrm{I}$ is the only critical point of U at which U has a positive definite Hessian, that is, U has a minimum [45].

Note that, since $\mathrm{x_d}(\tau) \in \mathbf{SO}(3)$, there exists $\Omega : \mathcal{I} \to \mathbf{so}(3)$ so that

$$\frac{d}{d\tau}\mathrm{x_d}(\tau) = \mathrm{x_d}(\tau)\Omega(\tau) \tag{13}$$

Then, following [42], the desired velocity field $V : \mathbf{SO}(3) \times \mathcal{I} \to T\mathbf{SO}(3) \times T\mathcal{I}$ can be derived as

$$\mathrm{V}(\bar{\mathrm{q}}) = \gamma_1(\bar{q}) \begin{pmatrix} \mathrm{E}(\bar{\mathrm{q}})\mathrm{x_d}(\tau)\Omega(\tau) \\ 1 \end{pmatrix} - \gamma_2(\bar{q}) \begin{pmatrix} \frac{1}{2\lambda'}(\mathrm{EPE}-\mathrm{P})\mathrm{x_d}(\tau) \\ 0 \end{pmatrix} \tag{14}$$

$$= \gamma_1(\bar{\mathrm{q}}) \begin{pmatrix} \mathrm{q}\Omega(\tau) \\ 1 \end{pmatrix} - \frac{\gamma_2(\bar{q})}{2\lambda'} \begin{pmatrix} \mathrm{q}\left[\mathrm{x_d}(\tau)^{\mathrm{T}}\mathrm{Pq} - \mathrm{q}^{\mathrm{T}}\mathrm{Px_d}(\tau)\right] \\ 0 \end{pmatrix} \tag{15}$$

Note that the speed of progression of the desired parameterized contour relative to the rate of convergence is determined by the relative magnitudes of $\gamma_1(\bar{q})$. *Self-pacing* exploits this relationship to yield better contour following characteristics. In particular, $\gamma_1(\bar{q})$ and $\gamma_2(\bar{q})$ are made to depend on the potential function $U(E(q,\tau))$ which measures the deviation of the current configuration from the desired location, so that when $U(E)$ is large, the velocity field prioritizes decreasing the tracing error. Consequently, when the tracking error is large, the desired trajectory x_d would progress at a slower speed. For instance, $\gamma_1(\bar{q})$, $\gamma_2(\bar{q})$ can be chosen as:

$$\gamma_1(\bar{q}) = \exp\left(-\nu\, U(\mathrm{E}(\mathrm{q},\beta))\right) \tag{16}$$

$$\gamma_2(\bar{q}) = 2 - \exp\left(-\nu\, U(\mathrm{E}(\mathrm{q},\beta))\right) \tag{17}$$

where $\nu > 0$ is the self-pacing parameter such that as ν increases, the emphasis on eliminating contour following error is also increased.

VI. Coupling with Virtual Reality

Virtual environment simulations with force-feedback are integrated in rehabilitation protocols not only for more engaging therapies, but also for ensured safety and ease modification of task parameters. Furthermore, force-feedback is indispensable for immersion and to have meaningful interactions with the virtual environment.

For the 3RPS-R forearm-wrist rehabilitation robot, a flight simulator is implemented for visual representation (see Figure 4). The plane is coupled to the end-effector of 3RPS-R and possesses the same metric space with the task space of the mechanism, that is, yaw-pitch-roll motions of the end-effector are mapped to same rotations of the plane. The task is to move the plane through a curved tunnel with a predetermined forward speed.

Force feedback is provided to the patient through implementation of a virtual tunnel coinciding with the visual representation of the tunnel and through PVFC guiding the patient within virtual tunnel. In particular, virtual tunnel defines forbidden regions in the workspace, by rendering a high stiffness "virtual wall" in the ϵ-neighborhood of the desired path. The virtual wall is implemented as cubic-damped spring using task space impedance control with orientation error metric [46], [47]. For patients with limited ability to control their limbs, PVFC is implemented inside the virtual tunnel to assist patient with completion of the task. In particular, a parameterized representation of the centerline defining the tunnel is used to construct the FrenetSerret frame of the curve, which governs the desired orientation along the tunnel. Then, a velocity field in $\mathbf{SO}(3)$ is constructed using suspension and self-pacing as discussed in Section V.

Type and power of the assistance may be customized with control parameters of the coupling controller (6), and exogenous signal (10), as well as velocity field generation parameters (equations (16) and (17).

VII. Experiment Results

Implementation of the controller is realized with the help of a desktop computer equipped with an I/O card running Quarc 2.0 on Matlab. Controllers are programmed in C for

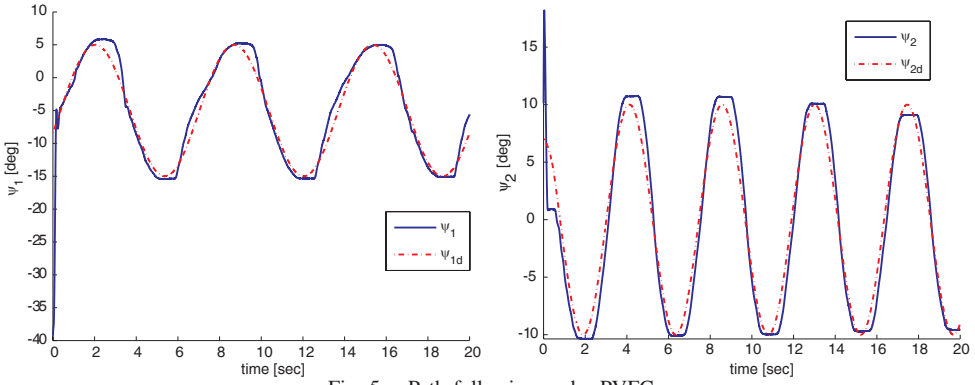

Fig. 5. Path following under PVFC

real-time implementation and the sampling frequency is set to 500 Hz. Since only position measurements are available via the encoders situated on the actuators, velocities are calculated using a nonlinear estimator based on the adaptive identification method, in an effort to reduce the numerical noise due to differentiation.

PVFC has been implemented for the 3RPS-R exoskeleton to minimize the "contour error" defined in $\mathbf{SO}(3)$. For simplicity, the desired path is parameterized by two sinusoids along ψ_1 and ψ_2 axis. This path does not impose any rotation about ψ_3. The initial conditions of the mechanism was intentionally offset from the desired configuration. Figure 5 presents contour tracking performance of the controller. Noting that when $\psi_3 = 0$, gravity field creates a moment in the positive ψ_2 direction, the tracking performance is quite satisfactory along both ψ_1 and ψ_2 axes. Slight overshoot can be observed on the ψ_2 axes due to unmodelled dynamics in the feedforward gravity compensation.

Figure 6 depicts the convergence characteristics and the total kinetic energy of the controlled system. The convergence is measured using the metric defined on $\mathbf{SO}(3)$, as given in equation 12. Exponential decay of the error metric can be observed within the first few instants of the experiment, while the convergence metric is kept near zero throughout the experiment. The kinetic energy of the augmented system is observed to decrease marginally due to friction inherent to the system. However, the rate of this decrease is low. If desired, extra energy can be introduced to the system via a feed-forward force. In this demonstration, no exogenous force is applied to the system.

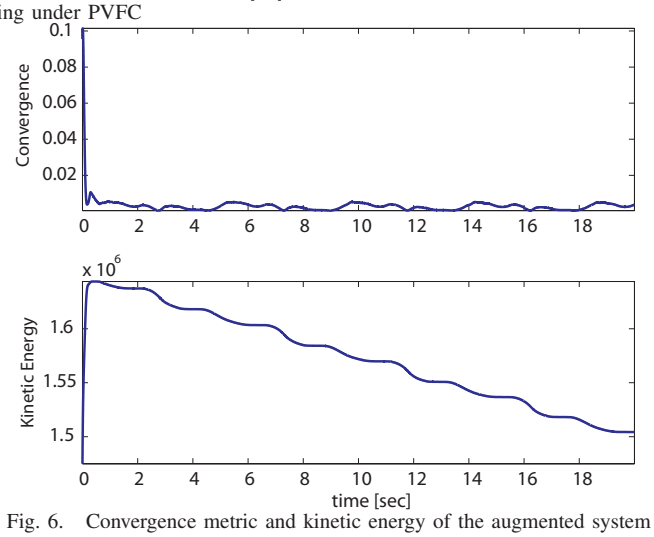

Fig. 6. Convergence metric and kinetic energy of the augmented system

VIII. Conclusions and Future Work

Design, implementation, and control of a parallel mechanism based exoskeleton aimed to deliver targeted therapeutic exercises to forearm and wrist are presented. During the design phase, different workspace and torque capabilities of human wrist about different motion axis are considered and a non-symmetrical 3RPS-R mechanism is selected as the underlying kinematic structure of the device. A prototype with optimal link lengths is implemented, that maximizes actuator utilization while simultaneously maximizing global isotropy and minimizing apparent inertia of the device. Workspace of the device is optimized considering the joint limits imposed by commercial spherical joints. Ergonomy and useability of the device is improved by featuring *open* semi-circular rings.

Path following controllers based on reduction of contour error is advocated over trajectory tracking controllers and PVFC approach is implemented to provide assistance to patients during contour following tasks, along with virtual tunnels implemented via impedance control at the task space of the device. The controllers are integrated into a virtual environment simulation with force-feedback, to render an engaging virtual flight simulator. Results of preliminary experiments with the device indicate the applicability and effectiveness of using PVFC for the 3RPS-R exoskeleton to deliver therapeutic movement exercises.

Future works include on-line generation of velocity fields based on data collected from the patients and clinical tests with stroke patients.

Acknowledgment

This work has been supported in part by FP7 Marie Curie International Reintegration Grant No: 203324.

References

[1] H. Krebs, B. Volpe, M. Aisen, and N. Hogan, "Increasing productivity and quality of care: Robot-aided neuro-rehabilitation," *Journal of Rehabilitation Research and Development*, vol. 37, no. 6, pp. 639–652, November/December 2000.

[2] H. Krebs, N. Hogan, M. Aisen, and B. Volpe, "Robot-aided neurorehabilitation," *IEEE Transactions on Rehabilitation Engineering*, vol. 6, no. 1, pp. 75–87, March 1998.

[3] J. Furusho, T. Kikuchi, K. Oda, Y. Ohyama, T. Morita, N. Shichi, Y. Jin, and A. Inoue, "A 6-DoF rehabilitation support system for upper limbs including wrists "Robotherapist" with physical therapy," in *Proceedings of the IEEE*. Netherlands: 10th International Conference on Rehabilitation Robotics, June 2007.

[4] J. Furusho, C. Li, X. Hu, N. Shichi, T. Kikuchi, A. Inoue, K. Nakayama, Y. Yamaguchi, and U. Ryu, "Development of a 6-DoF force display system using ER actuators with high-safety," in *VRCIA '06: Proceedings of the 2006 ACM international conference on Virtual reality continuum and its applications*, 2006, pp. 405–408.

[5] L. Dovat, O. Lambercy, Y. Ruffieux, D. Chapuis, R. Gassert, H. Bleuler, C. Teo, and E. Burdet, "A haptic knob for rehabilitation of stroke patients," in *Proceedings of the 2006 IEEE/RSJ*. China: International Conference on Intelligent Robots and Systems, October 2006.

[6] O. Lambercy, L. Dovat, V. Johnson, B. Salman, S. Wong, R. Gassert, T. Milner, T. Leong, and E. Burdet, "Development of a robot-assisted rehabilitation therapy to train hand function for activities of daily living," in *Proceedings of the 2007 IEEE*. Netherlands: International Conference on Rehabilitation Robotics, June 2007.

[7] L. Zhang, H. Park, and Y. Ren, "Developing an intelligent robotic arm for stroke rehabilitation," in *Proceedings of the IEEE*. Netherlands: 10th International Conference on Rehabilitation Robotics, June 2007.

[8] T. Nef, M. Mihelj, G. Colombo, and R. Riener, "ARMin - robot for rehabilitation of the upper extremities," in *Robotics and Automation. ICRA Proceedings 2006 IEEE International Conference on*, May 2006, pp. 3152–3157.

[9] A. Gupta, M. O'Malley, V. Patoglu, and C. Burgar, "Design, control and performance of RiceWrist: A force feedback wrist exoskeleton for rehabilitation and training," *IEEE Transactions on Robotics Research*, vol. 27, no. 2, pp. 233–251, February 2008.

[10] A. Sledd and M. O'Malley, "Performance enhancement of a haptic arm exoskeleton," in *Haptic Interfaces for Virtual Environment and Teleoperator Systems, 2006 14th Symposium on*, March 2006, pp. 375–381.

[11] A. Gupta and M. O'Malley, "Design of a haptic arm exoskeleton for training and rehabilitation," *IEEE/ASME Transactions on Mechatronics*, vol. 11, no. 3, pp. 280–289, June 2006.

[12] C. White, A. Schneider, and W. Brogan, "Robotic orthosis for stroke patient rehabilitation," in *Engineering in Medicine and Biology Society, 1993. Proceedings of the 15th Annual International Conference of the IEEE*, 1993.

[13] H. I. Krebs, B. T. Volpe, M. L. Aisen, W. Hening, S. Adamovich, H. Poizner, K. Subrahmanyan, and N. Hogan, "Robotic applications in neuromotor rehabilitation," *Robotica*, vol. 21, pp. 3–11, January 2003.

[14] R. Riener, L. Lunenburger, S. Jezernik, M. Anderschitz, G. Colombo, and V. Dietz, "Patient-cooperative strategies for robot-aided treadmill training: first experimental results," *Neural Systems and Rehabilitation Engineering, IEEE Transactions on*, vol. 13, no. 3, pp. 380–394, 2005.

[15] J. Emken, J. Bobrow, and D. Reinkensmeyer, "Robotic movement training as an optimization problem: designing a controller that assists only as needed," in *Rehabilitation Robotics, 2005. ICORR 2005. 9th International Conference on*, 2005.

[16] H. Vallery, A. Duschau-Wicke, and R. Riener, "Generalized elasticities improve patient-cooperative control of rehabilitation robots," in *Rehabilitation Robotics, 2009. ICORR 2009. IEEE International Conference on*, 2009, pp. 535 –541.

[17] M. Mihelj, "A novel paradigm for patient-cooperative control of upper-limb rehabilitation robots," *Advanced Robotics*, vol. 21, pp. 843–867(25), August 2007.

[18] T.-C. Chiu, "Coordination control of multiple axes mechanical system: Theory and experiments," Ph.D. dissertation, Univ. of California,, Dept. of Mechanical Engineering, Berkeley, CA, 1994.

[19] E. D. Tung, "Identification and control of high-speed machine tools," Ph.D. dissertation, Univ. of California,, Dept. of Mechanical Engineering, Berkeley, CA, 1993.

[20] K. H.I., "Rehabilitation robotics: Performance-based progressive robot-assisted therapy," *Autonomous Robots*, vol. 15, pp. 7–20(14), July 2003.

[21] L. L. Cai, A. J. Fong, C. K. Otoshi, Y. Liang, J. W. Burdick, R. R. Roy, and V. R. Edgerton, "Implications of assist-as-needed robotic step training after a complete spinal cord injury on intrinsic strategies of motor learning," *J. Neurosci.*, vol. 26, no. 41, pp. 10 564–10 568, 2006.

[22] A. Duschau-Wicke, J. von Zitzewitz, A. Caprez, L. Lunenburger, and R. Riener, "Path control: A method for patient-cooperative robot-aided gait rehabilitation," *Neural Systems and Rehabilitation Engineering, IEEE Transactions on*, vol. 18, no. 1, pp. 38 –48, 2010.

[23] Y. Li, V. Patoglu, and M. K. O'Malley, "Negative efficacy of fixed gain error reducing shared control for training in virtual environments," *ACM Trans. Appl. Percept.*, vol. 6, pp. 3:1–3:21, February 2009.

[24] P. Li and R. Horowitz, "Control of smart exercise machines. i. problem formulation and nonadaptive control," *Mechatronics, IEEE/ASME Transactions on*, vol. 2, no. 4, pp. 237 –247, December 1997.

[25] ——, "Passive velocity field control of mechanical manipulators," *Robotics and Automation, IEEE Transactions on*, vol. 15, no. 4, pp. 751 –763, August 1999.

[26] ——, "Passive velocity field control (pvfc). part i. geometry and robustness," *Automatic Control, IEEE Transactions on*, vol. 46, no. 9, pp. 1346 –1359, September 2001.

[27] D. Lee and P. Li, "Passive bilateral control and tool dynamics rendering for nonlinear mechanical teleoperators," *Robotics, IEEE Transactions on*, vol. 21, no. 5, pp. 936 – 951, October 2005.

[28] ——, "Passive bilateral feedforward control of linear dynamically similar teleoperated manipulators," *Robotics and Automation, IEEE Transactions on*, vol. 19, no. 3, pp. 443 – 456, June 2003.

[29] J. Moreno-Valenzuela, "On passive velocity field control of robot arms," in *Decision and Control, 2006 45th IEEE Conference on*, December 2006, pp. 2955 –2960.

[30] ——, "Velocity field control of robot manipulators by using only position measurements," *Journal of the Franklin Institute*, vol. 344, no. 8, pp. 1021 – 1038, 2007.

[31] J.-J. Slotine and W. Li, *Applied Nonlinear Control*. Prentice Hall, October 1990.

[32] N. Sadegh and R.Horowitz, "Stability and robustness analysis of a class of adaptive controllers for robotic manipulators," *International Journal of Robotics Research*, vol. 9, no. 3, pp. 74–92, June 1990.

[33] R. Ortega and M. Spong, "Adaptive motion control of rigid bodies," *Automatica*, Nov 1989.

[34] K. M. Lee and D. K. Shah, "Kinematic analysis of a three degrees-of-freedom in-parallel actuated manipulator," *IEEE Transactions on Robotics and Automation*, vol. 4, no. 3, pp. 354–360, 1988.

[35] C. H. Liu and S. Cheng, "Direct singular positions of 3RPS parallel manipulators," *ASME Journal of Mechanical Design*, no. 126, pp. 1006–1016, 2004.

[36] A. Gupta and M. K. O'Malley, "Design of a haptic arm exoskeleton for training and rehabilitation," *IEEE Transactions on Mechatronics*, vol. 11, no. 3, pp. 280–289, 2006.

[37] R. Unal and V. Patoglu, "Optimal dimensional synthesis of force feedback lower arm exoskeletons," in *IEEE International Conference on Biomedical Robotics and Biomechatronics*. BioRob, 2008.

[38] ——, "Optimal dimensional synthesis of a dual purpose haptic exoskeleton," in *Lecture Notes in Computer Science, Springer*, 2008.

[39] A. Erdogan, A. C. Satici, and V. Patoglu, "Reconfigurable force feedback ankle exoskeleton for physical therapy," in *in ASME/IFToMM International Conference on Reconfigurable Mechanisms and Robots*, June 2009.

[40] A. C. Satici, A. Erdogan, and V. Patoglu, "Design of a reconfigurable ankle rehabilitation robot and its use for the estimation of ankle impedance," June 2009.

[41] P. Li and R. Horowitz, "Passive velocity field control of mechanical manipulators," *Robotics and Automation, IEEE Transactions on*, vol. 15, no. 4, pp. 751 –763, aug 1999.

[42] ——, "Passive velocity field control (pvfc). part ii. application to contour following," *Automatic Control, IEEE Transactions on*, vol. 46, no. 9, pp. 1360 –1371, September 2001.

[43] D. E. Koditschek, *Dynamics and Control of Multibody Systems, Contemporary Mathematics*. American Mathematical Society, 1989, vol. 97, ch. The application of total energy as a Lyapunov function for mechanical control systems, pp. 131–157.

[44] D. Koditschek, "Total energy for mechanical control systems, in dynamics and control of multibody systems," *MS series on Contemporary Mathematics*, vol. 97, no. 4, pp. 131–157, June 1982.

[45] D. Chillingworth, J. Marsden, and Y. Wan, "Symmetry and bifurcation in three-dimensional elasticity, part i," *Arch. Rational Mech. Analy*, 1982.

[46] F. Caccavale, B. Siciliano, , and L. Villani, "The role of euler parameters in robot control," *Asian Journal of Control*, vol. 1, no. 1, pp. 25–34, March 199.

[47] B. Siciliano, L. Sciavicco, L. Villani, and G. Oriolo, *Robotics: Modelling, Planning and Control*. Springer, 2009.